Mucoadhesive thermosensitive hydrogel for the intra-tumoral delivery of immunomodulatory agents, in vivo evidence of adhesion by means of non-invasive imaging techniques

Katia Lemdani, Johanne Seguin, Christelle Lesieur, Chantal Al Sabbagh, Bich-Thuy Doan, Cyrille Richard, Claude Capron, Robert Malafosse, Vincent Boudy, Nathalie Mignet

Mucoadhesive thermosensitive hydrogel for the intra-tumoral delivery of immunomodulatory agents, in vivo evidence of adhesion by means of non-invasive imaging techniques

Katia Lemdani[1, 2, 3], Johanne Seguin[1], Christelle Lesieur[1], Chantal Al Sabbagh[1], Bich-Thuy Doan[6], Cyrille Richard[1], Claude Capron[2, 4], Robert Malafosse[2, 3], Vincent Boudy[1, 5], Nathalie Mignet*[1]

[1] UTCBS, Chemical and Biological Technologies for Health laboratory, CNRS, UMR 8258, INSERM U1267, Université de Paris, F-75006 Paris, France.

[2] EA4340 BCOH, Versailles University, Paris-Saclay University, Boulogne-92100, France.

[3] Department of Surgery and Oncology, Centre Hospitalier Universitaire Ambroise Paré, Assistance Publique-Hôpitaux de Paris, APHP

[4.] Immunology and hematology Department, Ambroise Paré Hospital Boulogne-92100, France.

[5] Pharmaceutical R&D Department, Agence Générale des Equipements et des Produits de Santé (AGEPS), Assistance Publique-Hôpitaux de Paris, AP-HP, 7, rue du Fer à moulin, F-75005 Paris, France.

[6] i-CLeHS, Chemistry for Life and Health Sciences laboratory, CNRS FRE2027, Chimie ParisTech, PSL, 75005 Paris, France

Key words

Thermosensitive gel, bioadhesivity, Dendritic cells, optical imaging, local immunomodulation, antitumor immune response.

***corresponding author:** nathalie.mignet@parisdescartes.fr

ABSTRACT

Intratumoral injection of biocompatible gels is increasingly used for the sustained delivery of drugs and vaccines to enhance the anti-cancer immune response. Granulocyte-macrophage colony stimulating factor (GM-CSF) has become an attractive adjuvant thanks to its ability to boost the antitumor immune response by inducing proliferation, maturation and migration of the dendritic-cells (DCs) and the differentiation of lymphocytes. Killed Mycobacteria, such as Heat-killed Mycobacterium tuberculosis (HKMT) have been used in several studies as TLR-2 agonist to increase maturation of DCs. In this study, we designed a mucoadhesive thermosensitive formulation for the local delivery of GM-CSF and HKMT in order to enhance DCs activation and improve the local antitumor immune response. This formulation was selected based on its elastic and mucoadhesive properties obtained thanks to rheological studies. More importantly, intratumoral residence time of the labelled gel and protein were evidenced by means of MRI and non invasive *in vivo* optical imaging. Then, the efficacy of the combination of immunomodulators loaded thermogel was demonstated *in vitro* and *in vivo*. The selected thermogel exibits rheological properties which confer a good elasticity and increased residence time of the immunostimulatory agents in the tumor, thus increasing the recruitment of DCs and T cytotoxic $CD8^+$ lymphocytes.

1. Introduction

Dendritic cells (DCs) based immunotherapy is a promising strategy in the treatment of cancer. DCs are the most important antigen presenting cells (APCs) involved in the regulation of innate and adaptive immunity and play a central role in the antitumor immune response (Sabado et al., 2017). Indeed, DCs mature quickly after exposure to stimuli and get the ability to migrate and activate naive lymphocytes into cytotoxic T cells (Banchereau et al., 2000).

In the past two decades, there has been a growing attempt to enhance immune responses by immunizing cancer patients with their own DCs that have been isolated and activated *ex vivo* (Gilboa, 2007). Several studies used *ex vivo* activated DCs of patients to treat various cancers such as kidney cancer, breast cancer, prostate cancer and colorectal carcinoma (Barth et al., 2010; Jähnisch et al., 2010). However, these clinical trials lost their interest because of the low effectiveness of DCs therapy related to their short viability and the suppressive immune environment of the tumor (Palucka et al., 2010). It was also shown that generated cells have a low *in vivo* migration capacity (Justus et al., 2014).

To overcome these limits, studies focused on direct *in vivo* targeting of DCs adjuvants such as TLR agonists, Cytokines or Interleukins (Tacken et al., 2007). Toll-like-receptors agonists, such as TLR2, TLR4, TLR7 or TLR9 were used to mature DCs *in vivo*. For example, CpG-DNA is a TLR 9 agonist which is used as an effective adjuvant to enhance immune response (Häcker et al., 2002). BCG (Bacilli of Calmette-Guerin) is a TLR-2/4 agonist approved as an adjuvant for non-invasive bladder cancer treatment (Alexandroff et al., 1999; Orihuela et al., 1987). TLR agonists administered by systemic pathways, were however, not well tolerated because they induce the release of high levels of cytokines, including IFNs, which are believed to cause most of the observed adverse reactions. In order to avoid these side effects, some studies demonstrated the interest of Heat killed mycobacteria as an adjuvant in cancer immunotherapy of multiple cancers (Stebbing et al., 2012).

Heat-killed (HK) Mycobacterium preparation has demonstrated immunotherapeutic effect for the treatment of advanced pancreatic cancer confirmed by a significant increase on the overall and progression-free survival of these patients (Dailey et al., 2006). Otherwise, heat-killed (HK)

Mycobacterium preparation has been shown to be safe and well tolerated among patients with stage III/IV melanoma (Stebbing et al., 2012). The immunological effect of these compounds was related to their abilities to induce innate immune reaction. Indeed, HK mycobacterium was reported to promote the development of $CD11c^+$ APCs in mice (Adams et al., 2004). *In vitro* stimulation of human blood cells with HK mycobacteria are able to modulate the expression of cell surface receptors on APCs and to stimulate Th-1 antitumor immune response (Fowler et al., 2012). A recent study showed that HK mycobacterium contribute to up-regulation of CD11c, CD80 and MHC class II expression on DCs via interaction with TLR2 and TLR1 receptors (Bazzi et al., 2017).

GM-CSF is critical to the regulation of anti-tumor immune responses by the activation of both innate and adaptive immunity through the activation of its heteromeric receptor CD116, present on multiple cell types (Gillessen et al., 2003; Mach et al., 2000; Qin et al., 1997). The cytoplasmic domains of the GM-CSF receptor beta chain are associated with the Janus kinase 2 (JAK2) whose phosphorylation triggers multiple intracellular signaling pathways, including STAT5 and MAPK.1. Then multiple GM-CSF target genes are constitutively activated, including the transcription factor PU.1, which regulates differentiation and maturation of macrophages (Hansen et al., 2008; Suh et al., 2005). Nevertheless, through *in situ* interactions in the tumors micro-environment, GM-CSF was described as an immune-independent tumor-promoting factor, increasing tumor cell growth, in multiple cancer types (Braun et al., 2004; Gutschalk et al., 2012; Mueller and Fusenig, 1999; Obermueller et al., 2004; Orlowski and Baldwin, 2002; Pei et al., 1999). High concentrations of GM-CSF can also result in immune suppression, explained through the mobilization of $Gr\text{-}1^+$ $CD11b^+$ Myeloid Derived Suppressor Cells (MDSC), inhibition of DCs migration and also down-regulation of DCs expression of the CCL19 receptor CCR7 and MHCII (Serafini et al., 2004).

Considering cytokines and TLR agonists adverse effects, *in situ* controlled release may be the most efficient way to create a microenvironment where host DCs can migrate, proliferate and differentiate (Kizana and Alexander, 2003). Encapsulation device is then a limiting step in the design of such strategy.

Intratumoral injection of biocompatible gels is increasingly used for the enhancement of drug delivery. Local delivery of immunomodulatory agents using biomaterials such as, microspheres or gel, has been proposed to enhance vaccine efficacy, avoid the side effects of the systemic delivery, and also protect encapsulated degradable molecules from denaturation. The first example showing the potential of this approach was given by Drissens et al. with pluronic entrapped GM-CSF (Wu et al., 2017). Poloxamers are FDA approved copolymers. Upon temperature and concentration increase, they undergo a sol-gel transition phase (Dumortier et al., 2006). This transition can be modified by addition of salts and viscous agents. Bioadhesives polymers have also been added to increase adhesion of the gel and its viscosity (Bhowmik et al., 2013). We have shown previously that addition of sataxiane in poloxamer based hydrogel allowed the release of salbutamol sublingually (Zeng et al., 2014). More recently, we found that *in situ* delivery of anticancer drugs could slightly reduce the size of the tumors allowing their removal via surgery (Mignet et al., 2015). In this study, we ought to deliver immunomodulators *in situ* within the tumor and evaluate the effect of the immunotherapy. As referred to the literature, the combination of immunomodulators chosen are expected to provide both DCs activation and maturation. The originality of the study lies in the demonstration of the residence time of the gel with or without bioadhesive agent by means of non-invasive MRI and *in vivo* optical imaging. The therapeutical possible effect was also pre-evaluated by following by *in vivo* optical imaging the release of a protein model imbedded within the gel. Finally, we evaluated if the improved viscosity and bioadhesivity properties of the immunostimulating thermogel resulted in an *in situ* immunomodulation effect evidenced by tumor volume regression and tumor infiltrating lymphocytes.

2. Material and methods

2.1. Materials, cell culture and animals

Poloxamer 407 (Kolliphor® P407) and xanthan gum (SATIAXANE CX 930) were purchased from BASF, France. Mucin from porcine stomach Type II (M2378-100G) and 4-nitrophenyl chloroformate were bought from Sigma Aldrich, France. Triethylamine, dichloromethane, methanol and DMSO were purchased from Carlo-Erba, France. GM-CSF (130-095-735) was bought from Miltenyi, France. Heat-killed Mycobacterium tuberculosis HKMT (tlrl-hkmt-1) was purchased from Invivogen, France. Antibodies against CD11c, CD86, CD80, were obtained from Becton Dickinson, France. Anti-CD3 was bought from Dako, France. Anti-CD4 was purchased from e-Bioscience, France. Anti-CD8 was bought from Neomarkers LabVision, US, and anti-Fox P3 from Abcam, France. Peroxidase/diaminobenzidine Rabbit PowerVision kit was purchased from ImmunoVision Technologies, US and Polink 2 plus HRP detection kit from GBI Labs, US. The transwell plates with 0.45 µm pore filters were bought from Sigma Aldrich, France.

CT26 colon adenocarcinoma cell line (CRL-2638) was purchased from American Type Culture Collection LGC Standards, France. Cells were cultured in Dulbecco's Modified Eagle Medium (DMEM, Gibco Life Technologies) containing 10% fetal bovine serum (FBS, Gibco Life Technologies, France), 100 µM of streptomycin, 100 U/mL of penicillin (Gibco Life Technologies, France).

8 week old female BALB/cJRj mice were obtained from Janvier laboratories, Le Genest de l'ile, France. Studies were conducted following the recommendations of the European Convention for the Protection of Vertebrate Animals Use for Experimentation and the local Ethics Committee on Animal Care and Experimentation, Paris Descartes university. (APAFIS # 11352).

2.2. Thermogels preparation

Thermogels were prepared according to the 'cold method' inspired from Smolka et al (Zeng et al., 2014). P407 21 % w/v (T-gel) was prepared by dispersing 2.1 g of P407 in 7ml of water (water for injection WFI, CDM Lavoisier, France). The preparation was left overnight at 4 °C until

clear solutions was obtained, and then the volume was completed to 10 mL. For the P407 / Satiaxane 21 / 0.1 % w/v (MT-gel) preparation, the Satiaxane 0.1 % solution was first prepared by dispersing 10 mg in 7 mL of sterile water, stirring continuously 30 min. at room temperature until complete dissolution. Then 2.1 g of P407 were added to the already swollen Satiaxane solution. The immunomodulatory thermogels (MTI-gel) were prepared at the day of experiment from the following composition P407 / Satiaxane 25 / 0.12 % w/v. GM-CSF (5µL, 1mg/ml water, 5µg) and/or HKMT (5µL, 2mg/ml NaCl 0.9%, 10µg) were added in 50 µL of the MT-gel and incubated at 4°C for 1 hour to get a complete solubilisation.

	P407	Satiaxane	GM-CSF +HKMT
T-gel	+	-	-
MT-gel	+	+	-
MTI-gel	+	+	+

Table. 1. Thermogels composition.

2.3. Rheology studies

Gelling temperature (Tg) of thermogel formulations was measured with a rheometer (Anton Paar model MCR 102, Courtaboeuf, France), fitted with a cone-plane mobile geometry (diameter = 50 mm; angle = 1) and a humidity cover to prevent influence of evaporation. A volume of 750 µL of thermogel was loaded on the support and then the mobile was descended to a distance equal to 0.1 mm from the support. Non-destructive oscillatory measurements at 1 Hz, performed in this study, allow one to obtain the elastic modulus (G'), the viscous modulus (G") and the phase angle (tan σ = G"/G'). The platewas heated at a rate of 1 °C/min from 20°C to 40°C. The sol-gel transition temperature was defined as the point where G0 began to shift to higher temperatures (Sandri et al., 2011). Each formulation was analyzed three times.

180 *2.4. In vitro muco-adhesion test*

181 Adhesion test was carried out using the comparison of the result obtained with a cone-plane
182 mobile coated or not by mucin (rheometer Anton Paar model MCR 102). A solution of Porcine
183 gastric mucin of type II (MUC2) (M2378, Sigma Aldrich) was prepared at 2 % in water . The
184 mobile was placed in this mucin solution and incubated at 37°C for 10 minutes. When the film
185 was dried, the mobile was settled and 550 µL of the sample loaded on the support of the
186 apparatus. The mobile was then brought down to a distance of 0.1 mm from the support. The
187 strength required to tear the gel was measured at 37°C (Detachment Force).

188

189 *2.5. P407 labelling with Cy5*

190 Hydroxyl groups of **poloxamer P407 (1)** were activated by reacting P407 (0.4 g) with 4-
191 nitrophenyl chloroformate (40 mg), triethylamine (30 µL) in dichloromethane (1.2 mL) (Fig. 4A).
192 The reaction was allowed to stir under argon overnight at room temperature. The **activated**
193 **polymer (2)** was precipitated in anhydrous diethyl ether and redissolved in methylene chloride.
194 This purification procedure was repeated three times and the activated P407 was then dried
195 under vacuum. To get **aminated P407 (3)**, activated P407 (0.2 g) dissolved in methanol (4 mL)
196 was reacted with ethylenediamine (0.1 g) overnight at room temperature and then precipitated
197 with anhydrous diethyl ether. Dried aminated P407 (10 mg) was finally reacted with Cy5-NHS (2
198 mg) in DMSO (1 mL) for 12 hours at room temperature. Byproducts were removed by dialysis
199 (MWCO 3500) against distilled water. Finally, **Cy5-P407 polymer (4)** (5 mg) was recovered by
200 lyophilization. To obtain Cy5-T-gel or Cy5-MT-gel, 1% of Cy5-P407 polymer was mixed with non-
201 labeled polymer in the formulation process.

202

203 *2.6. In vivo monitoring of the unlabelled thermogel by MRI*

204 Experiments were carried out at 7 T on a vertical imaging spectrometer fitted with an ultra
205 shielded refrigerated 300WB magnet (Bruker, Avance II, Wissembourg, France) equipped with a
206 whole-body 40 mm birdcage RF coil (Bruker) for mouse and Paravision 5.1 acquisition software.

For *in vivo* experiments, the mouse was positioned in a specific craddle maintaining the head via a face mask, which provided volatile anesthesia. The mice were anesthetized with 1.3% isoflurane (TEM, Bordeaux) in a mixture of oxygen-air (1:2, 1 L/min). The animal's temperature was monitored and controlled. Breath triggering was performed using a plastic sensor located on the mouse's thorax and the physiological monitoring for respiratory gating (SA Instruments Inc.). A 2D multislice GE sequence (TE = 5 ms) was first used for anatomical location of the tumor. The experimental parameters were as follows: hermitian pulse 3 ms, 30°, TR/TE 0.5s/3ms, with 20 slices of thickness of 1 mm, FOV = 3 x 3 cm. Images of 256 x 192 acquisition points were acquired, corresponding to an in-plane resolution of 120 µm x 157 µm. Then T2 weighted multiecho SE (RARE, 4 echoes) images with fat suppression were recorded (TR=3000ms, TE = 40ms). The experimental parameters were as follows: hermitian pulse 2 ms, TR/TE 1,5 s/40 ms, RARE factor 4, with a slice thickness of 1 mm, FOV = 3 x 3 cm. Images of 256 x 256 acquisition points were acquired, corresponding to an in-plane resolution of 117 µm x 117 µm. To understand *in vivo* residence time behaviour, CT26 tumor were bilaterally implanted in the flank of 8 weeks old BALB/cJRj females mice. Seven days after tumor implantation, T-gel or MT-gel (60 µL) was injected intratumorally with the help of a syringue (into the right and left tumor) of the mice (n=3). T2-weighted images were recorded, as described above, sequentially 30 min. and 6 h post thermogel injection to evidence the detection of the gel in hypersignal. The area of the gel was obtained after manual segmentation with image J software in the axial slice with the upper level of thermogel into the tumor. The percentage of gel area was calculated as function of the tumor area in the same axial slices.

2.7. In vivo monitoring of the labelled thermogel by optical imaging

Mice bearing CT26 tumor were anesthetized by i.p injection of a mixture 10 mg/kg Xylazine and 80 mg/kg Ketamine. Cy5-T-gel (60 µL) was injected on the left tumor whereas Cy5-MT-gel (60µL) was injected on the right tumor. Fluorescence signal was acquired with an epifluorescence system (Fluobeam camera, Fluoptics, France) at various time points post-injection. The signal was quantified over a region of interest (ROI) applied to the tumors using Image J software.

Results were expressed as the percentage (%) of the signal taken at t0 as regard to the percentage (%) of the signal at at time t, according to the formula:

$$\boldsymbol{Percent\ of\ signal}\ (\%\ \boldsymbol{of\ S}) = \frac{\boldsymbol{t}}{\boldsymbol{t0}} \times \mathbf{100}$$

2.8. In vivo monitoring of the protein release from the thermogel by optical imaging

Cy5-NHS was coupled to albumin, used as a model protein in PBS pH 7.4 for 30 min at room temperature. Free cyanine 5 was eliminated by ultracentrifugation at 12000 rpm, 4 °C during 10 min (6 times). Fluorescence and mass spectrometry confirmed the obtention of the labelled protein (Cyal) (M=67398 Da) (Lemdani et al., 2018).

Mice bearing CT26 tumor were anesthetized by i.p.injection of a mixture 10 mg/kg Xylazine and 100 mg/kg Ketamine. Cyal (0.5 mg/mL) embedded in the thermosensitive polymeric MT-gel (Cyal-MT-gel) was injected In the left tumor, whereas a solution of Cyal was injected In the right tumor. Fluorescence signal was acquired with a CDDi camera (Biospace Lab, France) at different time points post-injection. The quantification was performed over a region of interest (ROI) applied to the tumors using the M3 vision software. The release data were expressed as the percentage (%) of the signal taken at t0 as regard to the percent of the signal at at time t, according to the formula described in 2.7. part.

2.9. Cytotoxicity study

3LL Lewis lung carcinoma cell line (ATCC® CRL-1642™), B16 Melanoma cell line (ATCC® CRL-6323™), CT26 colorectal carcinoma cell line (ATCC® CRL-2638™) and murine NIH/3T3 (ATCC® CRL1658™) fibroblast cells were grown in DMEM medium containing 2 mL-glutamine, 10 % fetal bovine serum (3LL, B16 and CT26) or bovine serum (NIH/3T3), 100 U/mL penicillin, and 100 mg/mL streptomycin (37 °C, 5% CO_2). Cells in exponential growth were plated into 96-well plates at 20000 cells per well in 100 µL of culture medium. Twenty-four hours after plating, 60µL of T-gel, MT-gel or water were added on the cells, and incubated for 24 h at 37 °C and 5% CO_2.

After this exposure period, cell viability was assayed using the MTT test. The 3-(4, 5-dimethylthiazol-2-yl)-2, 5-diphenyltetrazolium bromide reagent (0.5 mg/mL) was added in each well and the plates were incubated 2 h at 37 °C. Then, the supernatant was carefully removed, and the formazan precipitate was solubilized in 100 µL of DMSO after 10 to 15 min agitation. Finally the absorbance was read at 562 nm with spectrophotometer (Plate reader Infinite 200 PRO - Life Sciences - Tecan) and the cell viability percent was calculated as regard to the value of the control (water for injectable preparation, 0.2 µm filtration).

2.10. In vitro Bone marrow dendritic cells generation

The bone marrow-derived dendritic cells (BMDCs) generation protocol was adapted from the procedure described by Lutz et al (Lutz et al., 1999). In brief, bone marrow from femurs and tibias of BALB/cJRj mice were taken under sterile conditions. The red blood cells were lysed with ammonium chloride buffer and the cells were cultured in RPMI medium supplemented with 10% FBS, 1 % PS, 1 % L-Glutamine and 20 ng/mL GM-CSF. Cultures were initiated by incubating 2 x 10^6 bone marrow cells in 10 mL of medium on 100 mm × 15 mm petri dishes (P5606-400EA, Sigma Aldrich. France). At day 3, an additional 7 mL of fresh complete medium was added. At day 6, the suspended BDMC cells were collected for further analysis.

2.11. In vitro activation of BMDCs

Empty gel (MT-gel) or MTI-gel containing either GM-CSF (5 µg) or HKMT (10 µg) or the combination of GM-CSF (5 µg) and HKMT (10 µg) were prepared. The transwell plates with 0.45 µm pore filters were used to study BMDCs migration and maturation. The thermogels were placed in the lower compartment of the transwell, whereas 2 x 10^5 BMDCs were seeded in the upper compartment. The cells which migrated into the lower compartment were collected 24h after incubation and labelled with rat anti-mouse PE CD11c (clone HL3), rat anti-mouse APC CD86 (clone GL1) and Hamster Anti-Mouse PerCP-Cy™5.5 CD80. The cells were analyzed with flow cytometry (FACS CANTO II, Becton Dickinson, France).

287 *2.12. Intratumoral injection of the MTI-gel*

288 BALB/cJRj 8 weeks old mice were injected in the right flank with 10^5 CT26 cells as previously
289 described (Seguin et al., 2013). After 11 days of inoculation, the mice were anesthetized under
290 Isoflurane mask. I-solution (GM-CSF-HKMT-Solution), MT-gel or MTI-gel were kept at 4°C and
291 were injected into the tumor using a 23G needle. The maximum volume to be administered
292 intratumorally was defined at 100 µL by workman et al (Workman et al., 2010). Injection of
293 various volume of hydrogel was tested from 30 -100 µL. The volume 60 µL was the most
294 adapted to include immunomodulators and prevent the reflux from the tumor site. The tumors
295 were measured every three days and their volume estimated with the formula:

$$Tumor\ Volume\ (mm^3) = (W^2 \times L)/2$$

296 The tumor growth is graphically represented as a function of time. When one of the mice was
297 sacrificed because it had reached an ethical limit point, the graphical representation of the
298 entire group was stopped. The median tumor volume of the control group (C) was determined
299 and when it reached approximately 250 mm^3, the median tumor volume of each treated group
300 (T) were measured, including zeros. The T/C value in percentage is calculated as follows:

$$T/C\ (\%) = \frac{Median\ tumor\ volume\ of\ the\ treated}{Median\ tumor\ volume\ of\ the\ control} \times\ 100$$

301

302 *2.13. Immunohistochemical study*

303 *2.13.1 Cell staining*

304 Freshly collected tumors were fixed in Zinc and embedded in paraffin, and sections (4 µm) were
305 realized. Paraffin sections were processed for heat-induced antigen retrieval, incubated with
306 rabbit anti-mouse CD3 antibody, monoclonal rat anti-CD4 and rabbit anti-mouse Fox P3
307 antibody. Staining was visualized by using the peroxidase/diaminobenzidine Rabbit PowerVision
308 kit (ImmunoVision Technologies). For CD8 immunohistochemistry, paraffin sections were
309 incubated with a rat monoclonal anti-CD8 (Neomarkers, LabVision). The membrane signal was

revealed with the Polink 2 plus HRP detection kit (GBI Labs). All slides were immunostained in cover plates the same day, to guarantee a standardized intensity of staining.

2.13.2. Quantification of T cells density

Each slide was examined using a microscope. The lymphocyte density was quantified on ten representative images realized with Leica Digital Microscopes (Leica DM 4000 B,Wetzlar, Germany) at x 20 magnification, with the help of image J software (Schneider et al., 2012). An original macro was created, which was dedicated to segment histologic parameters on the basis of contrast and color. Thus from original picture, a color deconvolution with DAB vectors was apply and the next step of analysis was performed on the red chanel obtained. This image was converted in 8-bit and the brightness and contrast was setting from 60 to 100. After binarization of the successive images 3 process was applied "Dilate, Fill Holes and Watershed" then the analysis of particles from 15-200 µm² (FOXP3) or 20-200 µm² (other cell type) was made.

2.14. Statistical analysis

Graph Pad Software was used to analyze data and determine statistical significance between groups. Data are shown as the means ± SEM. Mann-whitney test was used to compare the difference between two groups. One way anova test with Bonferroni posttest was used for mutiple comparaisons P values < 0.05 were considered significant. The symbol meaning : ns non significant $P > 0.05$, * $P \leq 0.05$, ** $P \leq 0.01$, *** $P \leq 0.001$.

3. Results

3.1. Formulation, mucoadhesion and cytotoxicity

3.1.1. Formulation

P407 concentration was adjusted to reach a gelation temperature (Tg) ranging between 18 and 25°C and a constant of elasticity G' above 10,000 Pa. The appropriate P407 concentration was fixed at 21 % w/v according to our previous study (Zeng et al., 2014). In order to endow the P407-based gel with bioadhesive properties, various amounts of Satiaxane gum (Sx) were added ranging from 0.05 up to 0.3 % w/v.The maximum proportion of Sx that can be added while remaining within the viscosity specification in the sol state was found to be 0.1 % w/v.

In table 2 are presented the measured parameters Tg, G', G'', and tanδ of P407 (T-gel) and P407-Sx (MT-gel) gels at 37°C. For both formulations, the Tg value was determined for tanδ = 1 and found to be very close to 21°C, interestingly about 16°C below the physiological temperature. At 37°C, i.e., in the gel state, G' was found higher than 10,000 Pa, reflecting strong elastic properties, moreover tanδ is close to 0, highlighting a strong solid behavior. Therefore, both formulations met the appropriate rheological specifications, without noticeable impact caused by the satiaxane gum in terms of gelling temperature or viscoelastic properties.

Composition (%w/v)	Tg (°C)	G' at 37°C (Pa)	G'' at 37°C	Tanδ at 37°C
T-gel P407 21%	21.0 ± 0.010	21400 ± 500	1100 ± 250	0.05 ± 0.001
MT-gel P407 21% Sx 0.1%	21.2 ± 0.005	21900 ± 150	600 ± 200	0.03 ± 0.001

Table. 2. Values of the temperature of gelification (Tg), the elastic modulus (G '), the viscous modulus (G'') and tanδ of the gel formulations. (n=3, mean ± SEM).

3.1.2. In vitro mucoadhesion

The main objective in adding Sx was to obtain a mucoadhesion *in vivo* and thus ensure longer residence time of the gel once injected in the tissue to be treated. To evaluate this property, a rheological method has been adapted from Ponchel et al (Ponchel et al., 1987). In order to evaluate the adhesiveness and the mucoadhesion of the thermogels, the mobile of the rheometer covered with a mucin film was put in contact with the support containing the gel (Fig. 1A). The obtained curves had a profile type IV characterized by four stages: cavitation, foam formation, elongation, and failure (Schmolka, 1972) (Fig. 1B). It appears in all conditions

359 that the normal force of cavitation reached 100 N and the normal force of elongation amounted
360 to 55 N. Only the duration of the elongation stage depended on the presence of Sx or mucin.
361 When the mobile was coated with mucin, the time to break the interaction increased by a factor
362 5 for T-gel (2.7 ± 0.6 s) and a factor 10 for the MT-gel (6.0 ± 1.6 s). As expected, the gel based on
363 P407 alone had a mucoadhesive character (Dumortier et al., 2006). The addition of Satiaxane
364 increased the *in vitro* mucoadherence by a factor 2 (Fig. 1C).

365 *3.1.3. In vitro cytotoxicity*

366 Prior evaluating the mucoadhesion of the thermogel *in vivo*, we ought to look for the toxicity of
367 the gel *in vitro* (Fig. 2). The effect of T-gel and MT-gel was evaluated on 3 tumor cell lines and 1
368 fibroblast cell line as regard to water, which is the solvent contained in the gel. No significant
369 difference was found between the formulations and water, indicating an absence of toxicity
370 related to the gel components.

371

372 3.1.4 *In vivo* mucoadhesion

373 In order to evaluate if mucoadhesion data obtained by rheometry could reflect a mucoadhesion
374 *in vivo*. We performed non-invasive longitudinal monitoring of the gel by MRI. T-gel and MT-gel
375 were injected in CT26 tumors grafted in the flank of mice. We showed in Fig. 3 that the gel could
376 be followed thanks to an hypersignal obtained by T2-MRI. The signal related to the water
377 confined within the gel was therefore taken as a signature of the thermogel. By this method, we
378 could evidence the effect of the mucoadhesive agent on the gel. Indeed, MT-gel could be
379 detected longer within the tumor area than T-gel. Two time-points illustrate this observation
380 (Fig. 3).

381 The difficulty in this experiment is that the signal of water is followed and multifactors might
382 occur, the release of water but also the swelling of the gel. A covalent label of the polymer
383 would lead to more reliable data to follow the gel. Therefore, to confirm that the residence time
384 of MT-gel was longer than the one of T-gel, we labelled poloxamer P407 with a fluorescent dye,
385 cyanine 5 (Cy5) in order to follow the gel by optical imaging. The labeling was realized in three

steps from commercially available dihydroxypoloxamer (P407) (Fig. 4A). The labeled polymer has the fluorescence characteristics of the Cy5 dye (λ emission = 640 nm in PBS) . To prepare fluorescent hydrogel (T-gel or MT-gel), one percent of the labeled polymer (4) was mixed with non-labeled polymer during the formulation process and the obtained sol was injected intratumorally. After intratumoral injection, we observed a similar level of fluorescence for both T and MT gel, however 24 h after the injection, a strong difference was noticeable with 54 % of the initial signal for T-gel and 65 % for the MT-gel. The calculated half-life indicated a value of 14.20 h for T-gel and 23.91 h for MT-gel, revealing a residence time increased by 1.7 fold when the gel was mucoadhesive. Based on rheological properties, *in vitro* mucoadherence results and *in vivo* residence in the tumor, the MT-gel formulation was selected for the evaluation of *in vitro* and *in vivo* bioactivity studies.

3.2. Bioactivity

3.2.1. In vivo release study of Cyal.

Cyanin-5 labelled albumin, also called Cyal and described in (Lemdani et al., 2018), was used as a model protein. The *in vivo* release of Cyalwas performed by optical imaging. Cyal loaded MT-gel was injected into the left tumor and Cyal solution in the right tumor of CT26 bearing mice. In Fig. 5, a decrease of the fluorescence signal of Cyal solution was observed few hours after injection with a total elimination at 24h. Fifty percent of the signal issued from the Cyal-MT-gel persisted long hours after injection. The half life and the area under the curve of Cyal-MT-gel was 19.2 h and 1565 % x h respectively as regard to 5.1 h and 1078 % x h for Cyal solution confirming a sustained released of protein *in vivo* using the thermogel.

3.2.2 In vitro DCs activation

To activate DCs, the immunostimulatory protein GM-CSF and the killed bacteria HKMT were entrapped within the MT-gel in order to form an immune stimulating thermogel (MTI-gel). The inclusion of these molecules within the gel did not alter the transition phase of the gel using

differential scanning calorimetry (DSC). No effect was found at the onset of micellization (Supplementary information Fig. S1). The capacity of non-entrapped HKMT to activate bone marrow-derived dendritic cells (BMDCs) as compared with a positive control LPS (lipopolysaccharide) was first tested. We found a similar level of $CD80^+$ (61.7 vs 50.8 %) and of $CD86^+$ (58.9 % vs 50.6 %) expression in HKMT and LPS conditions, respectively (Supplementary information Fig. S2).

After these preliminary tests, MT-gel, GM-CSF-MT-gel, HKMT-MT-gel or MTI-gel were deposited on the lower compartment of transwells. The DCs generated from bone marrow were seeded on the upper compartment (Fig. 6A). The cells which crossed the membrane of the transwell were collected and analyzed by flow cytometry for $CD80^+$ and $CD86^+$ activation markers. The fluorescence intensity quantified in Fig. 6B, showed a high expression of $CD86^+$ with the GM-CSF-MT-gel and MTI-gel conditions. The MT-gel and the HKMT-MT-gel did not induce any DCs activation. Interestingly, the expression of $CD80^+$ on DCs was higher for the combination of immune stimulating molecules. The double stained populations $CD11c^+$ $CD80^+$ and $CD11c^+$ $CD86^+$ are presented in Fig. 6C. The co-expression of both $CD80^+$ and $CD86^+$ on dendritic cells is necessary for T lymphocytes activation. Therefore, we found here that MTI-gel revealed a superior ability to induce dendritic cells maturation.

3.2.3. Local effect of intratumoral administration of the MTI-gel

To evaluate the effect of the immunostimulatory gel after intratumoral administration, we injected CT26 tumor bearing mice with MT-gel, a gel containing one or both immunomodulatory molecules (GM-CSF-MT-gel, HKMT-MT-gel and MTI-gel) or the two immunomodulatory molecules in solution (I-solution) (Fig. 7). The various treatments did not show a significant influence regarding the body weight apart from the control group which showed a decrease of weight 20 days after tumor implantation,due to the tumor toxicity (Fig. 7A). Regarding the tumor growth represented Fig. 7B, solely the complete treatment with both immunomodulatory molecules was able to decrease the tumor growth. In fact, a median tumor volume of 58.5 mm^3 for I-solution and 19.4 mm^3 for MTI-gel compared with 235,1 mm^3 for the control group were

441 measured at day 15 (Table 3). These data led to a growth delay of 5 days for the MT-gel
442 embedded one immunomodulatory molecules, 7 days for those two in solution and greater
443 than 31 days for the MTI-gel.

444

	Median tumor volume (mm^3, d15)	T/C % d15	Time for median tumor to reach 250 mm^3 (day)	T-C (day)
Control	235,1		15	
I-solution	58,8	25,01	22	7
MT-gel	82,5	35,09	20	5
GM-CSF-MT-gel	212	90,18	17	2
HKMT-MT-gel	65,9	28,01	20	5
MTI-gel	19,4	8,25	>31	>16

	MT-gel vs					GM-CSF-gel vs				HKMT-gel vs			MTI-gel vs	
Days	control	GM-CSF-gel	HKMT-gel	MTI-gel	I-solution	control	HKMT-gel	MTI-gel	I-solution	control	MTI-gel	I-solution	control	I-solution
8	ns	ns	ns	ns	ns	ns	ns	ns	ns	ns	ns	ns	ns	ns
11	ns	ns	ns	ns	ns	ns	ns	ns	ns	ns	ns	ns	ns	ns
13	ns	ns	ns	ns	ns	ns	ns	ns	ns	ns	ns	ns	ns	ns
15	ns	ns	ns	ns	ns	ns	ns	ns	**	ns	ns	ns	ns	ns
17	ns	ns	ns	ns	ns	***	ns	ns	**	ns	ns	ns	ns	ns
20	***	ns	ns	ns	ns	***	ns	ns	ns	***	ns	ns	***	ns

Table 3. Effect of thermogel intratumoral injection

Table 4. Statistical analysis of the effect of thermogel intratumoral injection. Two-way ANOVA with Bonferroni posttests was performed, n=6, ns non significant, * P<0.05, ** P <0.01, ***P <0.01

3.2.4. Local immune infiltration after MTI-gel intratumoral administration

In order to analyze the immune environment within intratumoral administration of the MTI-gel, CD3 cells, effector T cells (CD4+), cytotoxic T cells (CD8+), regulatory T cells (FoxP3) were analyzed with immunohistochemistry (Fig. 8A). We observed a significant increase of CD3 and

CD8 cell density on the tumor with injection of MTI-gel as compared to MT-gel. There was no difference on CD4, FoxP3 cell density on the two conditions (Fig. 8B).

4. Discussion

In this study, we proposed a mucoadhesive thermogel for the intratumoral delivery of GM-CSF and HKMT. These immunomodulatory agents are known to induce the recruitment and maturation of DCs, which are necessary to activate T cells and induce an effective immune response (Palucka and Coussens, 2016). Local immunomodulation has shown extensive interests these last years (Marabelle et al., 2017; Mazzolini et al., 2005; Narita et al., 2015; Park et al., 2018; Sangro et al., 2004; W. Tong et al., 2012). The interest of poly (ethylene oxide)–poly (propylene oxide)–poly (ethylene oxide) (PEO-PPO-PEO) triblock copolymers based gels for human use is now clearly established (Jeong et al., 2012). Among these, the poloxamer P407 is a FDA approved water-soluble polymer (Matthew et al., 2002). When dissolved in water at a specific range of concentration, poloxamer P407 exhibits thermosensitive properties attributed to its chemical structure which explain its widespread use as a drug delivery system for controlled release applications (Hoare and Kohane, 2008; Jeong et al., 2012).

Properties of bioadhesion can be provided to the gel by mucoadhesive agents for the purpose of extending the residence time at the injection site (Khutoryanskiy, 2011; Madsen et al., 1998). Based on our previous local delivery studies using P407 (Zeng et al., 2014), we chose to strenghten the residence time of the thermogel by the addition of mucoadhesive agents within the gel (Zeng et al., 2014). Satiaxane was chosen for the viscosity it will bring to the gel as well as its capacity to interact with mucins (Ceulemans et al., 2002). Adapted rheological studies were performed to quantify the bioadhesion by means of the gel failure upon destroying its interaction with mucin. Mucin was chosen as an adequate matrix overexpressed in colorectal tumors (Niv and Rokkas, 2018). Based on the rheological and mucoadhesion properties, the MT-gel was chosen, owning a fitting cohesiveness, hardness and mucoadhesion. In order to insure that these *in vitro* results would reflect a mucoadhesion *in vivo*, the residence time of the gel was evaluated by means of two non-invasive imaging techniques, MRI and optical imaging, post intratumoral injection. By both methods, we observed a persistence of the mucoadhesive gel.

Interestingly, MRI allowed the detection of confined water within the gel without any labelling. With this method, we could follow the early time after injection to evaluate the behavior of the gel and in particular its spilling. However, after few hours, other mechanisms interfer such as gel swelling and volume reduction. This internalisation and release of water of the gel impacts the MRI signal and would require more development to explain the signal related mechanism. Then, P407 was labelled with Cy5 for optical imaging studies. The migration of the labelled P407 from the gel could induce false data interpretation but it seems, that it remained within the gel as we could evidence that the MT-gel was still present 5 days after injection in the tumor.

Release studies and kinetic of gel stability are usually evaluated *in vitro* using flow-through method operated in open-loop mode capable of maintaining a continuous flow of fresh dissolution medium (Gao, 2009). However, data obtained are relative results based on the experimental conditions. In order to evaluate the gel elimination and protein release in relevant conditions, we performed these experiments *in vivo* using labelled protein. As regard to Cyal, only one Cy5 was grafted to avoid any aggregation of the protein and modification of its structure. This was controlled by means of flow field flow fractionation coupled with multi-angle light scattering (Salmon et al., 2019). Using optical imaging, we observed that the signal of Cy5 labelled protein incorporated in the mucoadhesive gel persisted 7 days after intratumoral injection.

Based on these results, we could therefore argue that the mucoadhesive thermogel studied present required qualities for local immunomodulation. Still, some parameters remain to be optimized such as the process of DCs maturation which is currently greater than 100 hours and a life expectancy of only few days for maturated DCs that migrate to lymph nodes (Sallusto and Lanzavecchia, 2002). Thus, a prolonged release of immunomodulatory agents on the tumor environment over 100 hours could improve the maturation of DCs and increase the proportion of migrated cells to the lymph nodes.

The effectiveness of DCs maturation is dependent on the bioactivity of the immunomodulatory agents after gel incorporation. We demonstrated the ability of the gel containing GM-CSF and HKMT to increase the maturation of DCs. Indeed, the expression of $CD86^{+}$/$CD80^{+}$ costimulatory

509 factors on maturated DCs was higher after incubation with the complete gel formulation as
510 compared to gel containing GM-CSF or HKMT alone. The expression of co-stimulatory factors is
511 necessary to activate naïve T cells (Madsen et al., 1998). It was demonstrated that $CD86^{+}$/$CD80^{+}$
512 expression by DCs is reduced in GM-CSF-deficient mice (Madsen et al., 1998). DCs interaction
513 with mycobacteria family is known to increase the surface density of molecules such as MHC II,
514 $CD80^{+}$, $CD86^{+}$, and IL-12 production that are involved in interaction with T cells (Sinha et al.,
515 2007).

516 The intratumoral administration of the immunomodulators in the gel led to an inhibition of
517 tumor growth, while the administration of a solution of these immunomodulatory agents
518 demonstrated minimal effects. Indeed, the injection of the solution in the tumor increased the
519 concentration of GM-CSF on the tumor microenvironment and probably caused the protein
520 leak into the circulatory system, which induced immunosuppressive effects as described by
521 several studies (Clive et al., 2010; Parmiani et al., 2007; Serafini et al., 2004). We also showed
522 that the local delivery of GMCSF alone was not sufficient to induce an immune response, the
523 combination of the immunomodulators was required to obtain a complete response. The
524 rational of GMCSF and HKMT combination is not demonstrated. In preclinical studies,
525 vaccination with a BCG-secreting GM-CSF showed an increased DCs maturation through CD11c
526 MHCII_ and CD11c CD11b F480 expressing cells and IFNɣ secreting T cells compared with the
527 use of the BCG alone. This vaccination resulted in the enhanced expression of co-stimulatory
528 molecules on DCs in the draining lymph nodes. The strategy combining BCG and GMCSF resulted
529 in an 10-fold increase in protection against disseminated M. tuberculosis (Ryan et al., 2007).
530 GM-CSF is expressed following infection with Mycobacterium tuberculosis and is necessary to
531 restrict M. tuberculosis growth in experimental models (Rothchild et al., 2017). Mycobacteria
532 increase GM-CSF mRNA and protein expression in a dose dependent manner. Secretion of GM-
533 CSF, mediated via the PI3-K, MEK1 and p38 MAPK-associated signaling pathway. Induction of
534 GM-CSF mRNA expression peaked 6 h after infection, and returning to its basal levels at 72 h
535 (Cho et al., 2013). This short constitutive expression kinetics of low level of GMCSF may explain
536 the failure of HKMT alone to induce an effective immune response in our study. In our recent
537 published study, we showed that association of radiofrequency with *in situ* modulation using

BCG and GM-CSF resulted in the complete cure of distal metastases (Lemdani et al., 2019). According to the obtained results in this study and in order to avoid BCG side effects, HKMT could be proposed to replace BCG in preclinical studies.

5. Conclusions

This study finally shows that *in situ* sustained delivery of HKMT and GMCSF related to the use of mucoadhesive poloxamer allows readjustment of the doses and dynamics of the two adjuvants needed for DCs recruitment and maturation. These results confirmed the need of a sustained delivery form to control the delivery of GM-CSF and avoid systemic side effects. We have shown a control of tumor volume mediated by cytotoxic T cells infiltration on the tumor with MTI-gel treatment. In human, involvement of tumor infiltration of T cells to obtain an antitumor immune response is considered to be predictive factor, associated with long-term survival of patients (Emile et al., 2017). Thus, the MTI-gel designed in this study could be a vector for the sustained release of immunomodulatory molecules in the tumor microenvironment to improve the antitumor immune response.

Author contributions

NM VB and RM designed the thermogel and managed the project. CL and CAS performed rheological studies. CR labelled the poloxamer with Cy5. BTD CL and JS did MRI experiments. KL and JS did *in vivo* experiments and IHC analyses. KL did the cellular *in vitro* tests. CC participated to flow cytometry analysis. KL RM JS and NM wrote and the manuscript. CL and VB participated to manuscript edition.

Acknowledgements

The authors would like to thank the LIOPA (the small animal optical imaging platform), the Animal facility of the faculty of pharmacy and ICM (cellular and molecular imaging platform) from UMS 3612 CNRS, Paris Descartes University, France. In vivo imaging was performed at the Life Imaging Facility of Paris Descartes University (PIV, Plateforme Imageries du Vivant), supported by France Life Imaging (grant ANR-11-INBS-0006), the Infrastructures Biologie-Santé and the GDR-AIM. The authors thank Olivia Bawa from ´Unité de pathologie expérimentale de l'IRCIV, Gustave Roussy, Villejuif, France' for IHC staining.

Conflict of interest

Authors declare that they have no conflict of interests**.**

Funding

This work was supported by grants from the 'Ligue contre le cancer', the association of research in digestive oncology (A.R.O.L.D) and the SATT IDF Innov

References and notes

Adams, V.C., Hunt, J.R.F., Martinelli, R., Palmer, R., Rook, G.A.W., Brunet, L.R., 2004. Mycobacterium vaccae induces a population of pulmonary CD11c+ cells with regulatory potential in allergic mice. Eur. J. Immunol. 34, 631–638. https://doi.org/10.1002/eji.200324659

Alexandroff, A.B., Jackson, A.M., O'Donnell, M.A., James, K., 1999. BCG immunotherapy of bladder cancer: 20 years on. Lancet 353, 1689–1694. https://doi.org/10.1016/S0140-6736(98)07422-4

Banchereau, J., Briere, F., Caux, C., Davoust, J., Lebecque, S., Liu, Y., Pulendran, B., Palucka, K., 2000. Immunobiology of dendritic cells. Annu. Rev. Immunol. 18, 767–811. https://doi.org/10.1146/annurev.immunol.18.1.767

Barth, R.J., Fisher, D.A., Wallace, P.K., Channon, J.Y., Noelle, R.J., Gui, J., Ernstoff, M.S., 2010. A randomized trial of ex vivo CD40L activation of a dendritic cell vaccine in colorectal cancer patients: Tumor-specific immune responses are associated with improved survival. Clin. Cancer Res. 16, 5548–5556. https://doi.org/10.1158/1078-0432.CCR-10-2138

Bazzi, S., Modjtahedi, H., Mudan, S., Achkar, M., Akle, C., Bahr, G.M., 2017. Immunomodulatory effects of heat-killed Mycobacterium obuense on human blood dendritic cells. Innate Immun. 23, 592–605. https://doi.org/10.1177/1753425917727838

Bhowmik, M., Kumari, P., Sarkar, G., Bain, M.K., Bhowmick, B., Mollick, M.M.R., Mondal, D., Maity, D., Rana, D., Bhattacharjee, D., Chattopadhyay, D., 2013. Effect of xanthan gum and guar gum on in situ gelling ophthalmic drug delivery system based on poloxamer-407. Int. J. Biol. Macromol. 62, 117–123. https://doi.org/10.1016/j.ijbiomac.2013.08.024

Braun, B., Lange, M., Oeckler, R., Mueller, M.M., 2004. Expression of G-CSF and GM-CSF in human meningiomas correlates with increased tumor proliferation and vascularization. J. Neurooncol. 68, 131–140. https://doi.org/https://doi.org/10.1023/B:NEON.0000027751.87894.f0

Ceulemans, J., Vinckier, I., Ludwig, A., 2002. The use of xanthan gum in an ophthalmic liquid dosage form: Rheological characterization of the interaction with mucin. J. Pharm. Sci. 91, 1117–1127. https://doi.org/10.1002/jps.10106

Cho, J.E., Park, S., Lee, H., Cho, S.N., Kim, Y.S., 2013. Mycobacterium tuberculosis-induced expression of granulocyte-macrophage colony stimulating factor is mediated by PI3-K/MEK1/p38 MAPK signaling pathway. BMB Rep. 46, 213–218. https://doi.org/10.5483/BMBRep.2013.46.4.200

Clive, K.S., Tyler, J.A., Clifton, G.T., Holmes, J.P., Mittendorf, E.A., Ponniah, S., Peoples, G.E., 2010. Use of GM-CSF as an adjuvant with cancer vaccines: beneficial or detrimental? Expert Rev. Vaccines 9, 519–525. https://doi.org/10.1586/erv.10.40

Dailey, L.A., Jekel, N., Fink, L., Gessler, T., Schmehl, T., Wittmar, M., Kissel, T., Seeger, W., 2006. Investigation of the proinflammatory potential of biodegradable nanoparticle drug delivery systems in the lung. Toxicol. Appl. Pharmacol. 215, 100–108. https://doi.org/https://doi.org/10.1016/j.taap.2006.01.016

Dumortier, G., Grossiord, J.L., Agnely, F., Chaumeil, J.C., 2006. A review of poloxamer 407 pharmaceutical and pharmacological characteristics. Pharm. Res. 23, 2709–2728. https://doi.org/10.1007/s11095-006-9104-4

Emile, J.F., Julié, C., Le Malicot et al. 2017. Prospective validation of a lymphocyte infiltration prognostic test in stage III colon cancer patients treated with adjuvant FOLFOX. Eur. J. Cancer 82, 16–24. https://doi.org/10.1016/j.ejca.2017.04.025

Fowler, D.W., Copier, J., Wilson, N., Dalgleish, A.G., Bodman-Smith, M.D., 2012. Mycobacteria activate γδ T-cell anti-tumour responses via cytokines from type 1 myeloid dendritic cells: A mechanism of action for cancer immunotherapy. Cancer Immunol. Immunother. 61, 535–547. https://doi.org/10.1007/s00262-011-1121-4

Gao, Z., 2009. In Vitro Dissolution Testing with Flow-Through Method: A Technical Note. AAPS

628 PharmSciTech 10, 1401–1405. https://doi.org/10.1208/s12249-009-9339-6
629 Gilboa, E., 2007. Review series DC-based cancer vaccines. J. Clin. Invest. 117, 1195–1203.
630 https://doi.org/10.1172/JCI31205.the
631 Gillessen, S., Naumov, Y.N., Nieuwenhuis, E.E.S., Exley, M.A., Lee, F.S., Mach, N., Luster, A.D., Blumberg,
632 R.S., Taniguchi, M., Balk, S.P., Strominger, J.L., Dranoff, G., Wilson, S.B., 2003. CD1d-restricted T
633 cells regulate dendritic cell function and antitumor immunity in a granulocyte-macrophage colony-
634 stimulating factor-dependent fashion. Proc. Natl. Acad. Sci. 100, 8874–8879.
635 https://doi.org/10.1073/pnas.1033098100
636 Gutschalk, C.M., Yanamandra, A.K., Linde, N., Meides, A., Depner, S., Mueller, M.M., 2012. GM-CSF
637 enhances tumor invasion by elevated MMP-2, -9, and -26 expression. Cancer Med. 2, 117–129.
638 https://doi.org/10.1002/cam4.20
639 Häcker, G., Redecke, V., Häcker, H., 2002. Activation of the immune system by bacterial CpG-DNA.
640 Immunology 105, 245–251. https://doi.org/10.1046/j.0019-2805.2001.01350.x
641 Hansen, G., Hercus, T.R., McClure, B.J., Stomski, F.C., Dottore, M., Powell, J., Ramshaw, H., Woodcock,
642 J.M., Xu, Y., Guthridge, M., McKinstry, W.J., Lopez, A.F., Parker, M.W., 2008. The Structure of the
643 GM-CSF Receptor Complex Reveals a Distinct Mode of Cytokine Receptor Activation. Cell 134, 496–
644 507. https://doi.org/10.1016/j.cell.2008.05.053
645 Hoare, T.R., Kohane, D.S., 2008. Hydrogels in drug delivery: Progress and challenges. Polymer (Guildf).
646 49, 1993–2007. https://doi.org/10.1016/j.polymer.2008.01.027
647 Jähnisch, H., Füssel, S., Kiessling, A., Wehner, R., Zastrow, S., Bachmann, M., Rieber, E.P., Wirth, M.P.,
648 Schmitz, M., 2010. Dendritic Cell-Based Immunotherapy for Prostate Cancer. Clin. Dev. Immunol.
649 2010, 1–8. https://doi.org/10.1155/2010/517493
650 Jeong, B., Kim, S.W., Bae, Y.H., 2012. Thermosensitive sol-gel reversible hydrogels. Adv. Drug Deliv. Rev.
651 64, 154–162. https://doi.org/10.1016/j.addr.2012.09.012
652 Justus, C.R., Leffler, N., Ruiz-Echevarria, M., Yang, L. V., 2014. In vitro Cell Migration and Invasion Assays.
653 J. Vis. Exp. 1–8. https://doi.org/10.3791/51046
654 Khutoryanskiy, V. V, 2011. Advances in mucoadhesion and mucoadhesive polymers. Macromol. Biosci.
655 11, 748–64. https://doi.org/10.1002/mabi.201000388
656 Kizana, E., Alexander, I., 2003. Cardiac Gene Therapy: Therapeutic Potential and Current Progress. Curr.
657 Gene Ther. https://doi.org/10.2174/1566523034578249
658 Lemdani, K., Mignet, N., Boudy, V., Seguin, J., Oujagir, E., Bawa, O., Peschaud, F., Emile, J.F., Capron, C.,
659 Malafosse, R., 2019. Local immunomodulation combined to radiofrequency ablation results in a
660 complete cure of local and distant colorectal carcinoma. Oncoimmunology 8, 1–14.
661 https://doi.org/10.1080/2162402X.2018.1550342
662 Lemdani, K., Salmon, H., Gahoual, R., Bessodes, M., Scherman, D., Houzé, P., Seguin, J., Mignet, N., 2018.
663 Assessment of the targeting specificity of fluorescent albumin conceived as a preclinical agent of
664 the liver function. Nanoscale 10, 21151–21160. https://doi.org/10.1039/C8NR04163F
665 Lutz, M.B., Kukutsch, N., Ogilvie, A.L.J., Roßner, S., Koch, F., Romani, N., Schuler, G., 1999. An advanced
666 culture method for generating large quantities of highly pure dendritic cells from mouse bone
667 marrow. J. Immunol. Methods 223, 77–92. https://doi.org/10.1016/S0022-1759(98)00204-X
668 Mach, N., Gillessen, S., Wilson, S.B., Sheehan, C., Mihm, M., Dranoff, G., 2000. Differences in Dendritic
669 Cells Stimulated in Vivo by Tumors Engineered to Secrete Granulocyte-Macrophage Colony-
670 stimulating Factor or Flt3-Ligand. Cancer Res. 60, 3239–3246.
671 Madsen, F., Eberth, K., Smart, J.D., 1998. A rheological examination of the mucoadhesive/mucus
672 interaction: The effect of mucoadhesive type and concentration. J. Control. Release 50, 167–178.
673 https://doi.org/10.1016/S0168-3659(97)00138-7
674 Marabelle, A., Tselikas, L., de Baere, T., Houot, R., 2017. Intratumoral immunotherapy: Using the tumor
675 as the remedy. Ann. Oncol. 28, xii33-xii43. https://doi.org/10.1093/annonc/mdx683

Matthew, J.E., Nazario, Y.L., Roberts, S.C., Bhatia, S.R., 2002. Effect of mammalian cell culture medium on the gelation properties of Pluronics F127. Biomaterials 23, 4615–4619. https://doi.org/https://doi.org/10.1016/S0142-9612(02)00208-9

Mazzolini, G., Alfaro, C., Sangro, B., Feijoó, E., Ruiz, J., Benito, A., Tirapu, I., Arina, A., Sola, J., Herraiz, M., Lucena, F., Olagüe, C., Subtil, J., Quiroga, J., Herrero, I., Sádaba, B., Bendandi, M., Qian, C., Prieto, J., Melero, I., 2005. Intratumoral injection of dendritic cells engineered to secrete interleukin-12 by recombinant adenovirus in patients with metastatic gastrointestinal carcinomas. J. Clin. Oncol. 23, 999–1010. https://doi.org/10.1200/JCO.2005.00.463

Mignet, N., Boudy, V., Seguin, J., Scherman, D., 2015. Gelling compositions for treating malignant tumors and/or preventing tumor recurrence. EP15306426.

Mueller, M.M., Fusenig, N.E., 1999. Constitutive expression of G-CSF and GM-CSF in human skin carcinoma cells with functional consequence for tumor progression. Int. J. Cancer 83, 780–789. https://doi.org/10.1002/(SICI)1097-0215(19991210)83:6<780::AID-IJC14>3.0.CO;2-C

Narita, M., Kanda, T., Abe, T., Uchiyama, T., Iwafuchi, M., Zheng, Z., Liu, A., Kaifu, T., Kosugi, S., Minagawa, M., Itoh, K., Takahashi, M., 2015. Immune responses in patients with esophageal cancer treated with SART1 peptide-pulsed dendritic cell vaccine. Int. J. Oncol. 46, 1699–1709. https://doi.org/10.3892/ijo.2015.2846

Niv, Y., Rokkas, T., 2018. Mucin Expression in Colorectal Cancer (CRC). J. Clin. Gastroenterol. Publish Ah, 1. https://doi.org/10.1097/mcg.0000000000001050

Obermueller, E., Vosseler, S., Fusenig, N.E., Mueller, M.M., 2004. Cooperative autocrine and paracrine functions of granulocyte colony-stimulating factor and granulocyte-macrophage colony-stimulating factor in the progression of skin carcinoma cells. Cancer Res. 64, 7801–7812. https://doi.org/10.1158/0008-5472.CAN-03-3301

Orihuela, E., Herr, H.W., Pinsky, C.M., Whitmore, W.F., 1987. Toxicity of lntravesical BCG and Its Management in Patients With Superficial Bladder Tumors ED. Cancer 60, 326–333. https://doi.org/https://doi.org/10.1002/1097-0142(19870801)60:3<326::AID-CNCR2820600309>3.0.CO;2-5

Orlowski, R.Z., Baldwin, A.S., 2002. NF-kappaB as a therapeutic target in cancer. Trends Mol. Med. 8, 385–9. https://doi.org/https://doi.org/10.1016/S1471-4914(02)02375-4

Palucka, A.K., Coussens, L.M., 2016. The Basis of Oncoimmunology. Cell 164, 1233–1247. https://doi.org/10.1016/j.cell.2016.01.049

Palucka, K., Ueno, H., Roberts, L., Fay, J., Banchereau, J., 2010. Dendritic cells: are they clinically relevant? Cancer J. 16, 318–324. https://doi.org/10.1097/PPO.0b013e3181eaca83

Park, C.G., Hartl, C.A., Schmid, D., Carmona, E.M., Kim, H.-J., Goldberg, M.S., 2018. Extended release of perioperative immunotherapy prevents tumor recurrence and eliminates metastases. Sci. Transl. Med. 10, eaar1916. https://doi.org/10.1126/scitranslmed.aar1916

Parmiani, G., Castelli, C., Pilla, L., Santinami, M., Colombo, M.P., Rivoltini, L., 2007. Opposite immune functions of GM-CSF administered as vaccine adjuvant in cancer patients. Ann. Oncol. 18, 226–232. https://doi.org/10.1093/annonc/mdl158

Pei, X.H., Nakanishi, Y., Takayama, K., Bai, F., Hara, N., 1999. Granulocyte, granulocyte-macrophage, and macrophage colony-stimulating factors can stimulate the invasive capacity of human lung cancer cells. Br. J. Cancer 79, 40–46. https://doi.org/10.1038/sj.bjc.6690009

Ponchel, G., Touchard, F., Duchêne, D., Peppas, N.A., 1987. Bioadhesive analysis of controlled-release systems. II. Time-Dependent bioadhesive stress in poly(acrylic acid)-containing systems. J. Control. Release 5, 129141. https://doi.org/10.1016/0168-3659(87)90005-8

Qin, Z., Noffz, G., Mohaupt, M., Blankenstein, T., 1997. Interleukin-10 prevents dendritic cell accumulation and vaccination with granulocyte-macrophage colony-stimulating factor gene-modified tumor cells. J. Immunol. 159, 770–6.

724 Rothchild, A.C., Stowell, B., Goyal, G., Nunes-Alves, C., Yang, Q., Papavinasasundaram, K., Sassetti, C.M.,
725 Dranoff, G., Chen, X., Lee, J., Behar, S.M., 2017. Role of Granulocyte-Macrophage Colony-
726 Stimulating Factor Production by T Cells during Mycobacterium tuberculosis Infection. MBio 8,
727 e01514-17. https://doi.org/10.1128/mBio.01514-17
728 Ryan, A.A., Wozniak, T.M., Shklovskaya, E., O'Donnell, M.A., Fazekas de St. Groth, B., Britton, W.J.,
729 Triccas, J.A., 2007. Improved Protection against Disseminated Tuberculosis by Mycobacterium bovis
730 Bacillus Calmette-Guerin Secreting Murine GM-CSF Is Associated with Expansion and Activation of
731 APCs. J. Immunol. 179, 8418–8424. https://doi.org/10.4049/jimmunol.179.12.8418
732 Sabado, R.L., Balan, S., Bhardwaj, N., 2017. Dendritic cell-based immunotherapy. Cell Res. 27, 74–95.
733 https://doi.org/10.1038/cr.2016.157
734 Sallusto, F., Lanzavecchia, A., 2002. Sallusto - DC on T cell responses. Arthritis Res. 4, S127–S132.
735 Salmon, H., Gahoual, R., Houzé, P., Ibrahim, T., Bessodes, M., Scherman, D., Seguin, J., Mignet, N., 2019.
736 Europium labeled lactosylated albumin as a model workflow for the development of
737 biotherapeutics. Nanomedicine Nanotechnology, Biol. Med. 18, 21–30.
738 https://doi.org/10.1016/j.nano.2019.02.011
739 Sandri, G., Bonferoni, M.C., Ferrari, F., Rossi, S., Fante, C. Del, Perotti, C., Caramella, A.G. and C., 2011. An
740 In Situ Gelling Buccal Spray Containing Platelet Lysate for the Treatment of Oral Mucositis. Curr.
741 Drug Discov. Technol. https://doi.org/http://dx.doi.org/10.2174/157016311796799017
742 Sangro, B., Mazzolini, G., Ruiz, J., Herraiz, M., Quiroga, J., Herrero, I., Benito, A., Larrache, J., Pueyo, J.,
743 Subtil, J.C., Olagüe, C., Sola, J., Sádaba, B., Lacasa, C., Melero, I., Qian, C., Prieto, J., 2004. Phase I
744 trial of intratumoral injection of an adenovirus encoding interleukin-12 for advanced digestive
745 tumors. J. Clin. Oncol. 22, 1389–1397. https://doi.org/10.1200/JCO.2004.04.059
746 Schmolka, I.R., 1972. Artificial Skin I. Preparation and Properties od Pluronic F-127 Gels for Treatment of
747 Burns. J. Biomed. Mater. Res. 6, 571–582. https://doi.org/10.1371/journal.pone.0100632
748 Schneider, C.A., Rasband, W.S., Eliceiri, K.W., 2012. NIH Image to ImageJ: 25 years of Image Analysis HHS
749 Public Access. Nat. Methods 9, 671–675. https://doi.org/10.1038/nmeth.2089
750 Seguin, J., Doan, B., Latorre Ossa, H., Jugé, L., Gennisson, J., Tanter, M., Scherman, D., Chabot, G.G.,
751 Mignet, N., 2013. Evaluation of Nonradiative Clinical Imaging Techniques for the Longitudinal
752 Assessment of Tumour Growth in Murine CT26 Colon Carcinoma. Int. J. Mol. Imaging 2013, 983534.
753 https://doi.org/10.1155/2013/983534
754 Serafini, P., Carbley, R., Noonan, K.A., Tan, G., Bronte, V., Borrello, I., 2004. High-Dose Granulocyte-
755 Macrophage Colony – Stimulating Factor – Producing Vaccines Impair the Immune Response
756 through the Recruitment of Myeloid Suppressor Cells 6337–6343.
757 Sinha, A., Salam, N., Gupta, S., Natarajan, K., 2007. Mycobacterium tuberculosis and dendritic cells:
758 Recognition, activation and functional implications. Indian J. Biochem. Biophys. 44, 279–288.
759 Stebbing, J., Dalgleish, A., Gifford-Moore, A., Martin, A., Gleeson, C., Wilson, G., Brunet, L.R., Grange, J.,
760 Mudan, S., 2012. An intra-patient placebo-controlled phase I trial to evaluate the safety and
761 tolerability of intradermal IMM-101 in melanoma. Ann. Oncol. 23, 1314–1319.
762 https://doi.org/10.1093/annonc/mdr363
763 Suh, H.-S., Kim, M.-O., Lee, S.C., 2005. Inhibition of Granulocyte-Macrophage Colony-Stimulating Factor
764 Signaling and Microglial Proliferation by Anti-CD45RO: Role of Hck Tyrosine Kinase and
765 Phosphatidylinositol 3-Kinase/Akt. J. Immunol. 174, 2712–2719.
766 https://doi.org/10.4049/jimmunol.174.5.2712
767 Tacken, P.J., De Vries, I.J.M., Torensma, R., Figdor, C.G., 2007. Dendritic-cell immunotherapy: From ex
768 vivo loading to in vivo targeting. Nat. Rev. Immunol. 7, 790–802. https://doi.org/10.1038/nri2173
769 Tong, W., Senzer, A., Cerullo, N. Smyth Templeton, V., Hemminki, N., Nemunaitis, A., 2012. Oncolytic
770 Viruses for Induction of Anti-Tumor Immunity. Curr. Pharm. Biotechnol. 13, 1750–1760.
771 https://doi.org/10.2174/138920112800958913

Workman, P., Aboagye, EO., Balkwill F., Balmain, A.? Bruder, G., Chaplin, DJ., Double JA., Everitt, J., Farningham, DA., Glennie, MJ., Kelland, LR., Robinson, V., Stratford, IJ.,Tozer, GM., Watson, S., Wedge, SR., Eccles, SA., 2010. Guidelines for the welfare and ise of animals in cancer research. Br. J. Cancer, 101, 1555-1577. https:// doi: 10.1038/sj.bjc.6605642

Wu, F., Dai, L., Geng, L., Zhu, H., Jin, T., 2017. Practically feasible production of sustained-release microspheres of granulocyte-macrophage colony-stimulating factor (rhGM-CSF). J. Control. Release 259, 195–202. https://doi.org/10.1016/j.jconrel.2017.04.004

Zeng, N., Dumortier, G., Maury, M., Mignet, N., Boudy, V., 2014. Influence of additives on a thermosensitive hydrogel for buccal delivery of salbutamol: Relation between micellization, gelation, mechanic and release properties. Int. J. Pharm. 467, 70–83. https://doi.org/10.1016/j.ijpharm.2014.03.055

Figures caption

Fig. 1. *In vitro* mucoadhesion test. (A) Mucoadhesion tests were carried out using a Rheometer (Anton Paar rheometer, model MCR 102, fitted with a 50 mm plane-plane mobile geometry) as described in methods (B) Detachment curves profile (C) Detachment curves of P407 (T-gel) and P407-Sx (MT-gel) formulations without (-) or in the presence of mucin (+) as function of time (n=3).

Fig. 2. Cell viability after exposure to H_2O (Control), T-gel or MT-gel of 3LL, B16, CT26 and NIH3T3 Cell lines. Data was expressed by Mean ± SEM (n = 6), $P > 0.05$ ns ,Two-way ANOVA with Bonferroni posttests was realized with GraphPad prism software.

Fig. 3. (A) *In vivo* T2-weighted MRI images of CT26 tumors 0.5h. (up) and 6 h (down) after injection of T-gel (left) and MT-gel (right). (B) Quantification of the thermogel area inside the tumor (%, Mean ± SEM, n=4). $P > 0.05$ ns, Two-way ANOVA with Bonferroni posttests was realized with GraphPad prism software.

Fig. 4. Synthesis of the labelled polymer and kinetic of elimination. (A) Synthetic procedure to label the poloxamer 4. i) Poloxamer P407 is first activated to dinitrophenyl carbonate polymer 2. ii) The activated polymer is then converted to diaminocarbamate 3. iii) Finally cyanine labeled poloxamer 4 is recovered after reaction with Cy5-NHS. (B) *In vivo* fluorescence imaging of injected mice, the right tumor received Cy5-T-gel, the left tumor received Cy5-MT-gel. (C) Longitudinal monitoring of the labelled gels when mucoadhesive (black circles dots) or not (white circles dots) in CT26 tumor model (n=6, mean ± SEM, nonlinear regression one phase exponential decay; $P > 0.05$ ns, Two-way ANOVA with Bonferroni posttests).

Fig. 5. Release kinetic of cyanine labelled protein from the mucoadhesive thermosensitive gel *in vivo*. (A) *In vivo* fluorescence imaging of injected mice at time 0, 2, 6 and 24h after injection. (R) The right tumor received Cyal solution and (L) the left tumor received Cyal-MT-gel. (B) Longitudinal monitoring of labelled protein release when injected as a mucoadhesive

thermosensitive gel (Black squares) or as an aqueous solution (white squares) in CT26 tumor model. The fluorescence signal quantification were expressed as the percentage (%) of the signal taken at t0 as regard to the the signal percent at time t (n=4, mean ± SEM, non linear regression biphasic fit, P > 0.05 ns, Two-way ANOVA with Bonferroni posttests).

Fig. 6. *In vitro* activation of BMDC within the immunomodulatory gel. (A) Schematic representation of the experiment. (B) Flow cytometry quantification of fluorescence intensity of V450-$CD80^+$ and APC-$CD86^+$ expression in MT-gel (white bar), GM-CSF-MT-gel (clear grey bar), HKMT-MT-gel (dark grey bar) and MTI-gel (dark bar) conditions. (C) $CD86^+$ and $CD80^+$ populations gated on $CD11c^+$ in the different conditions (n=5). Two-way ANOVA with Bonferroni posttests was done with GraphPad prism software.

Fig. 7. Effect of intratumoral administration of MTI-gel. (A) Difference in body weight after intratumoral injection for the Control (clear triangle), GM-CSF-MT-gel (clear diamond), HKMT-MT-gel (clear circle), I-solution (dark diamond), MT-gel (clear square) and MTI-gel (dark square) groups. Tumor growth after administration of those groups. Two-way ANOVA with Bonferroni posttests was performed, n=6, * P<0.05, ** P <0.01, ***P <0.01.

Fig. 8. (A) Representative images of the CD3, CD4, CD8 and FOXP3 immunostaining of CT26 tumor. Tumors from control, MT-gel and MTI-gel groups were removed 15 days after injection and fixed for further analysis. The black scale represents 50 µm. (B) Quantification of lymphocytes density on the tumor using macro image J as described on materials and methods; clear grey box represents the MT-gel group and dark grey box represents MTI-gel group. Mann-Whitney test, n=4, # P<0.05, ***P <0.01.

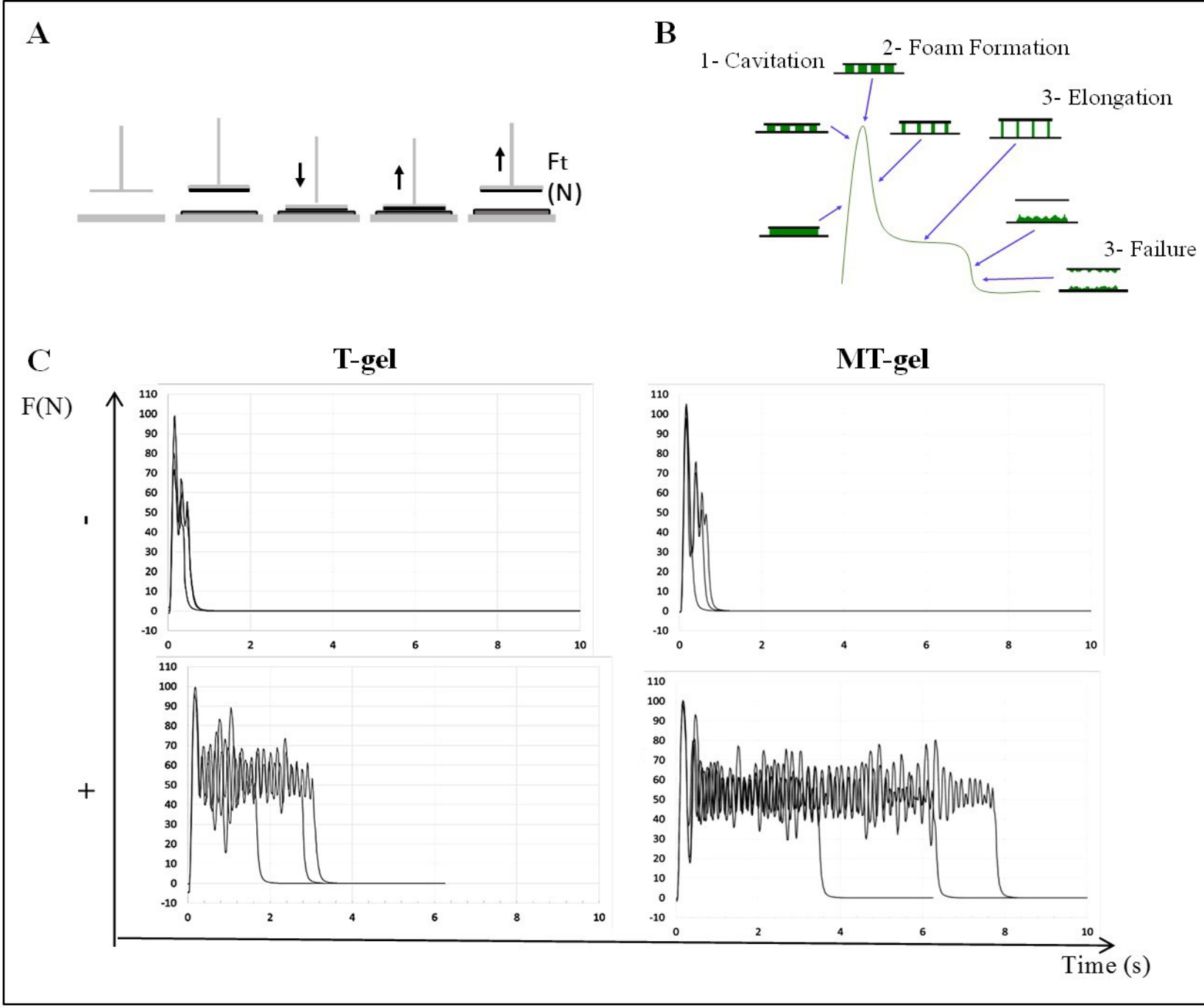
A
Ft
(N)
B
1- Cavitation
2- Foam Formation
3- Elongation
3- Failure
C
T-gel
MT-gel
F(N)
-
+
Time (s)

Fig. 1.

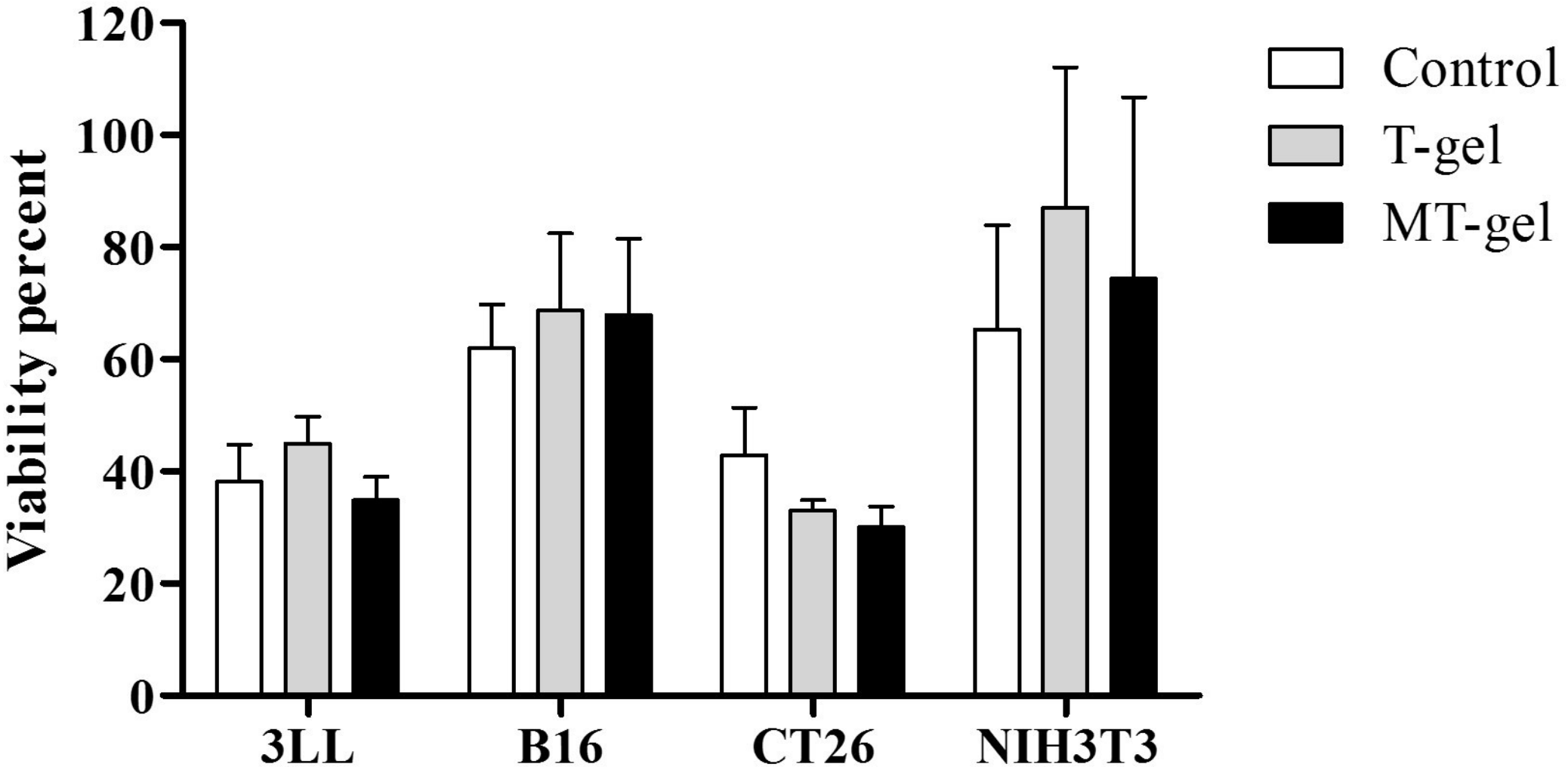
120
100
80
60
40
20
0
Viability percent
3LL
B16
CT26
NIH3T3
Control
T-gel
MT-gel

Fig. 2.

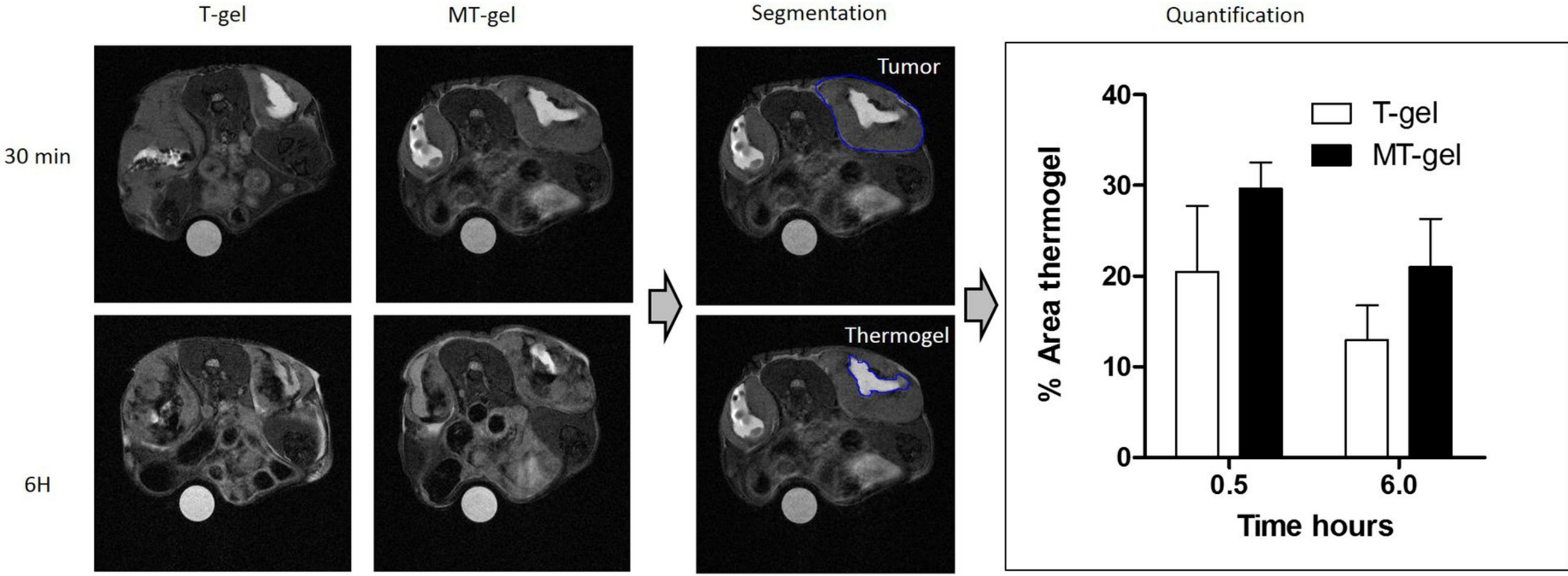
T-gel
MT-gel
Segmentation
Quantification
30 min
6H
Tumor
Thermogel
% Area thermogel
40
30
20
10
0
T-gel
MT-gel
0.5
6.0
Time hours

Fig. 3.

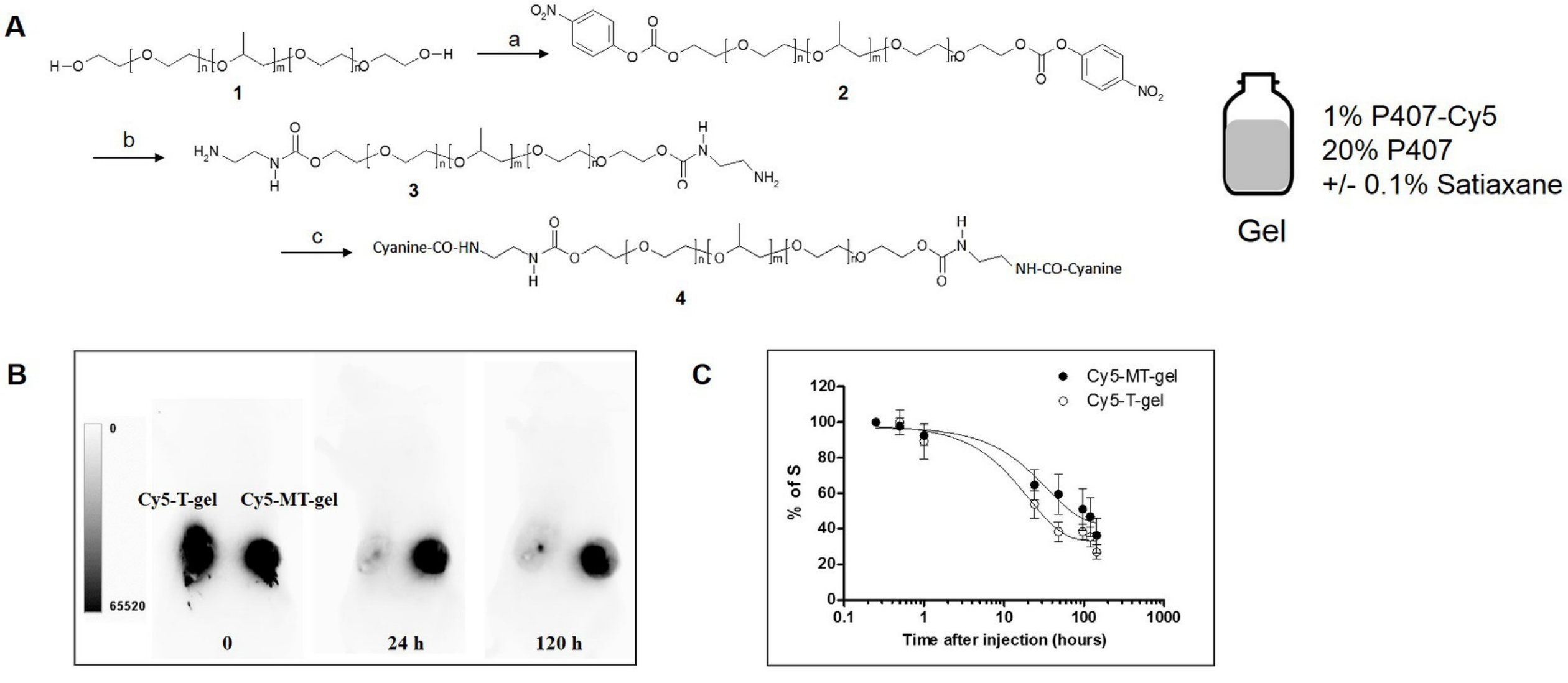
A
a
b
c
1
2
3
4
Cyanine-CO-HN
NH-CO-Cyanine
Gel
1% P407-Cy5
20% P407
+/- 0.1% Satiaxane
B
0
65520
Cy5-T-gel
Cy5-MT-gel
0
24 h
120 h
C
Cy5-MT-gel
Cy5-T-gel
% of S
Time after injection (hours)

Fig. 4.

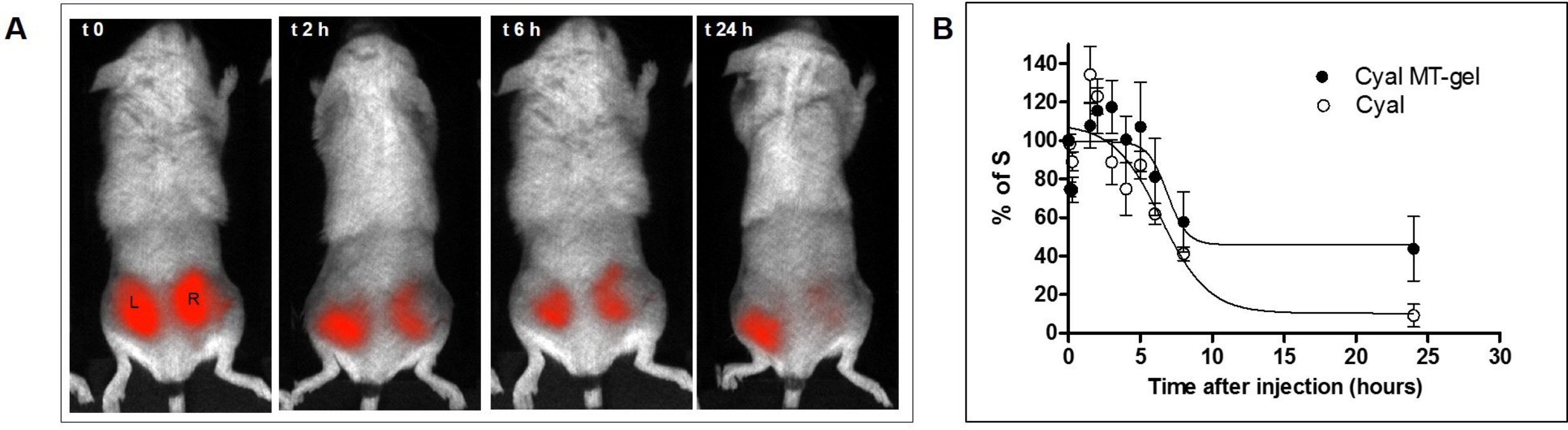
A
t 0
t 2 h
t 6 h
t 24 h
L
R
B
Cyal MT-gel
Cyal
% of S
Time after injection (hours)
0
20
40
60
80
100
120
140
0
5
10
15
20
25
30

Fig. 5.

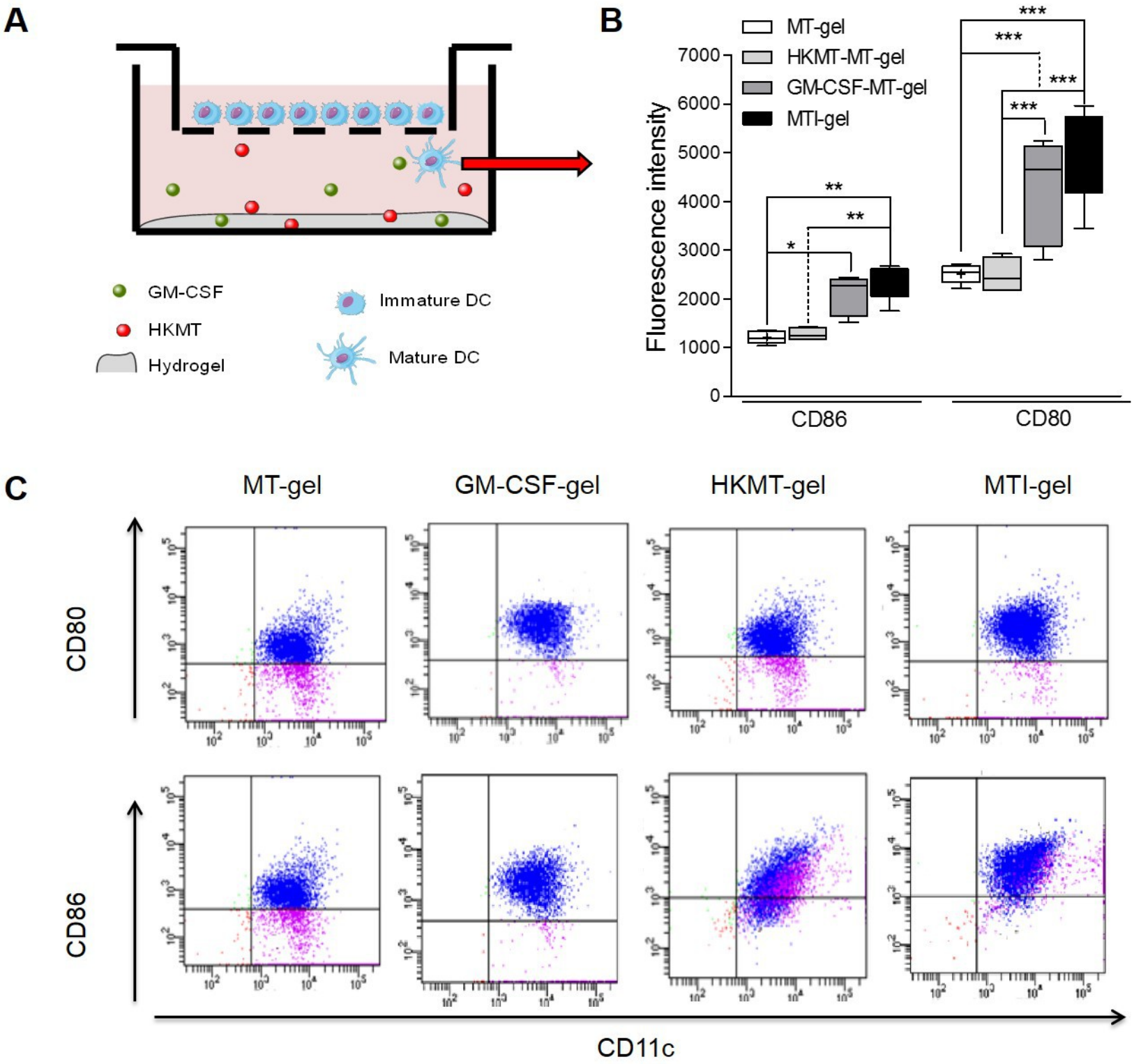
A
GM-CSF
HKMT
Hydrogel
Immature DC
Mature DC
B
MT-gel
HKMT-MT-gel
GM-CSF-MT-gel
MTI-gel
Fluorescence intensity
7000
6000
5000
4000
3000
2000
1000
0
CD86
CD80
C
MT-gel
GM-CSF-gel
HKMT-gel
MTI-gel
CD80
CD86
CD11c

Fig. 6.

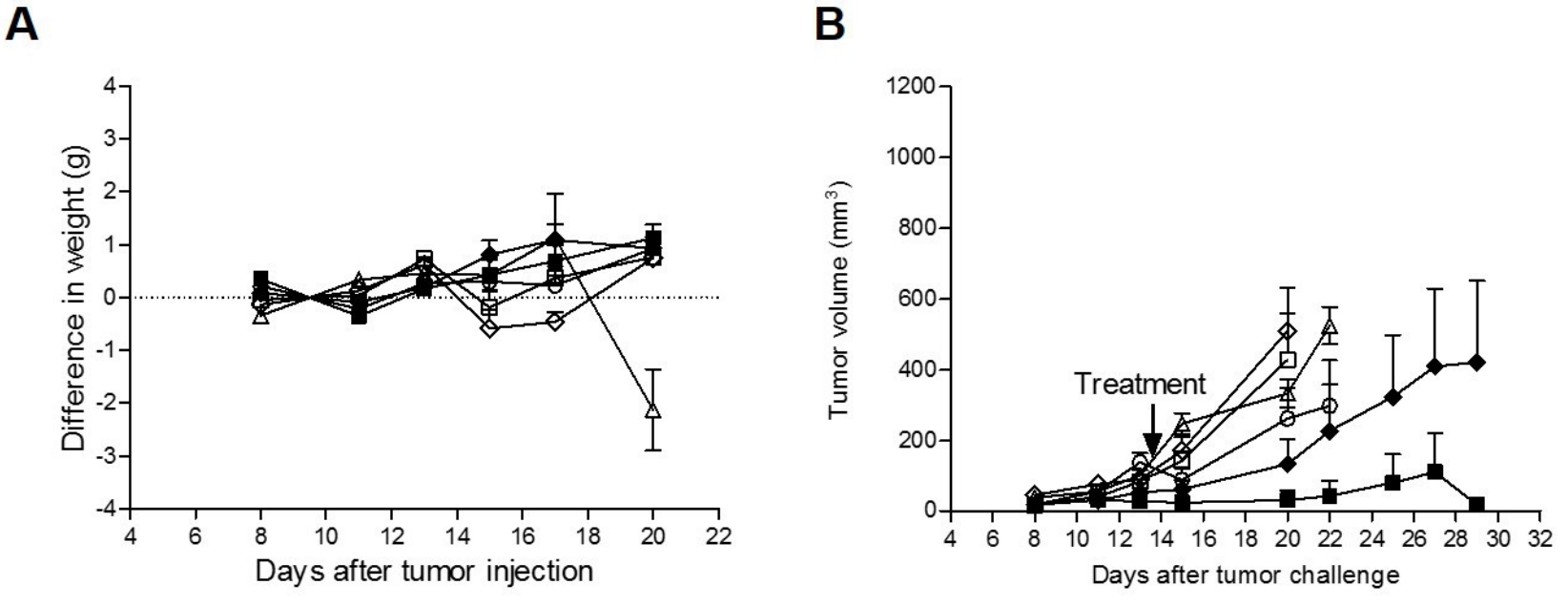
A
Difference in weight (g)
4
3
2
1
0
-1
-2
-3
-4
4
6
8
10
12
14
16
18
20
22
Days after tumor injection
B
Tumor volume (mm3)
1200
1000
800
600
400
200
0
Treatment
4
6
8
10
12
14
16
18
20
22
24
26
28
30
32
Days after tumor challenge

Fig. 7.

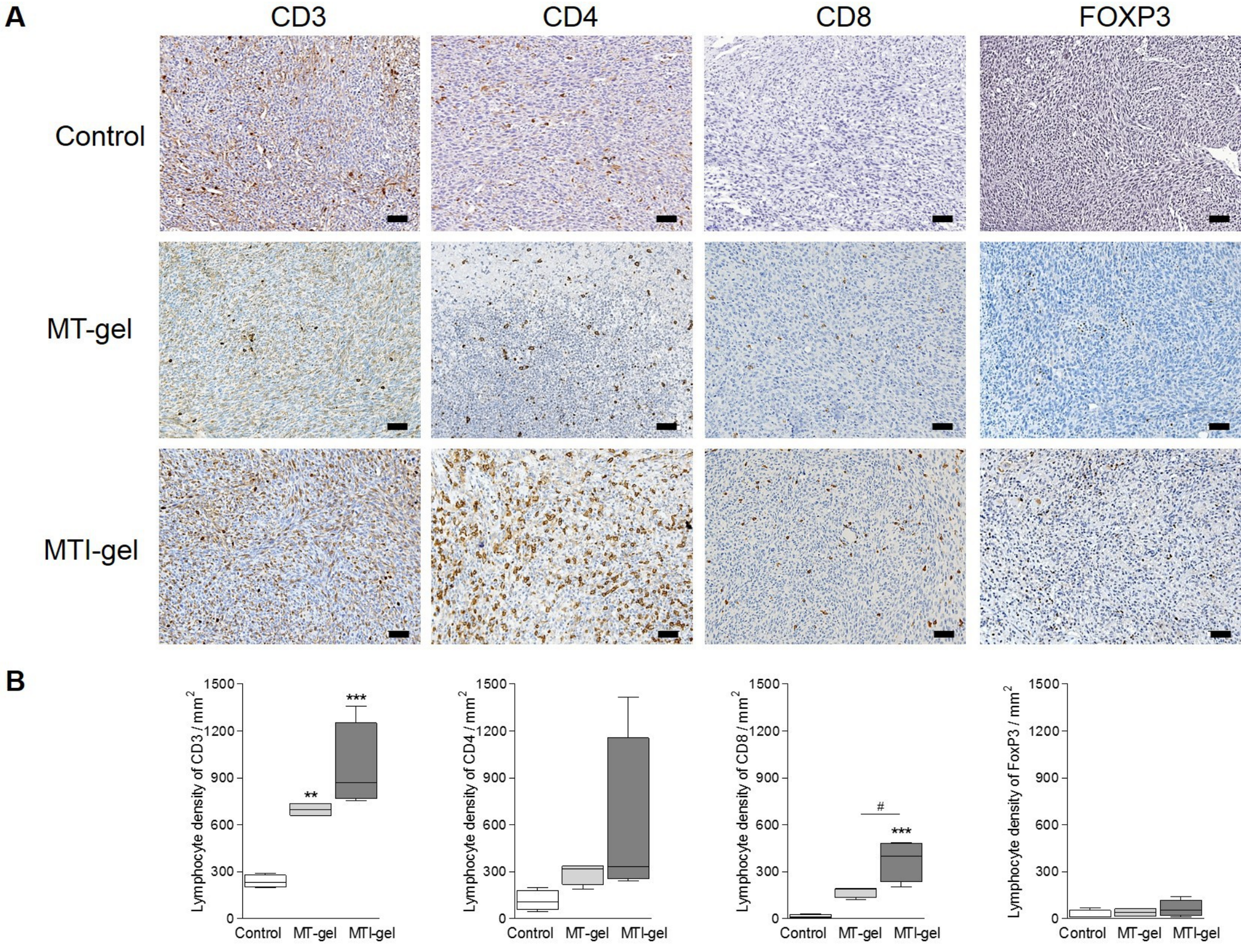
A
CD3
CD4
CD8
FOXP3
Control
MT-gel
MTI-gel
B
Lymphocyte density of CD3 / mm2
Lymphocyte density of CD4 / mm2
Lymphocyte density of CD8 / mm2
Lymphocyte density of FoxP3 / mm2
1500
1200
900
600
300
0
**
***
#
Control
MT-gel
MTI-gel

Fig. 8.

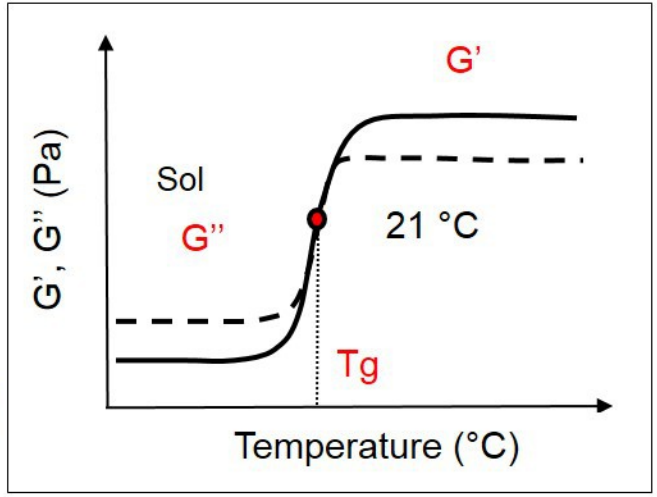

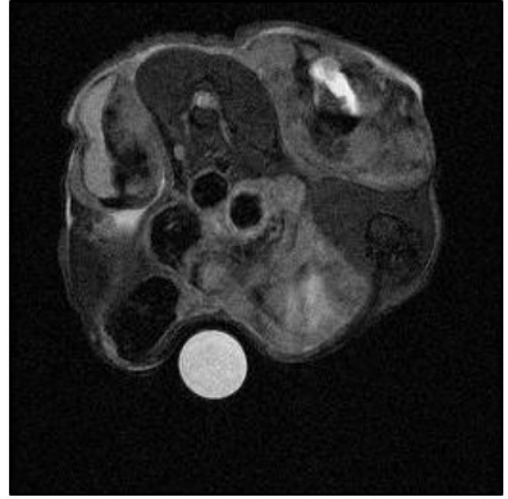

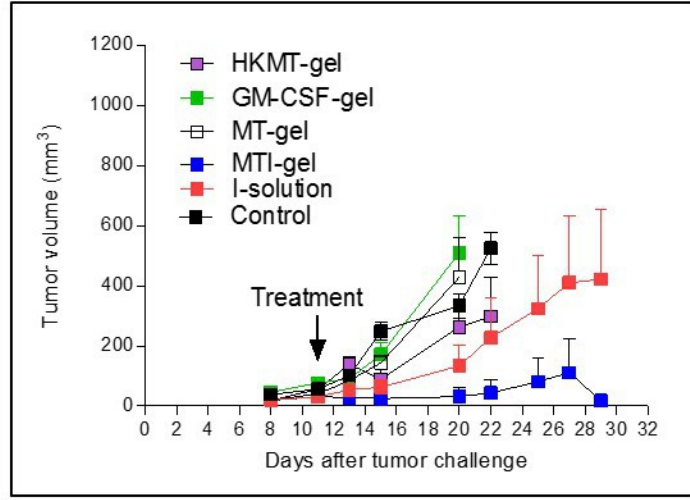

Gel

Gelification temperature

Gel residence

In vivo effect

Mucoadhesion

Protein residence time

Lymphocyte recruitement